Probing adsorption of water and DMF in UiO-66(Zr) using solid-state NMR

Florian Venel, Christophe Volkringer, Olivier Lafon, Frederique Pourpoint

Probing adsorption of water and DMF in UiO-66(Zr) using solid-state NMR

Florian Venel,[a] Christophe Volkringer,[a] Olivier Lafon,[a] Frédérique Pourpoint*[a]

a. *Univ. Lille, CNRS, Centrale Lille, Univ. Artois, UMR 8181 – UCCS – Unité de Catalyse et Chimie du Solide, 59000 Lille, France*
*corresponding author : frederique.pourpoint@centralelille.fr

The UiO-66(Zr) is one of the metal-organic frameworks (MOFs) with the highest thermal and chemical stability. Water and dimethyl formamide (DMF) play an important role in the crystallization of this MOF. Here we investigate using ^{1}H and ^{13}C NMR the adsorption of water and DMF in UiO-66(Zr) and notably the hydrogen bonds between these guest molecules and Zr–OH terminal groups of the metal clusters. We also report the selective deuteration of Zr–OH and aromatic hydrogen atoms of UiO-66(Zr).

The zirconium-based terephthalate UiO-66(Zr) ($Zr_6O_4(OH)_4(bdc)_6$, with bdc = 1,4-benzenedicarboxylate) is one of the most employed metal-organic frameworks (MOFs)[1], because of its high surface area (1187 $m^2.g^{-1}$) as well as its outstanding thermal and chemical stability compared to most of known MOFs[2]. In particular, this MOF remains stable when heated up to 450 °C or when exposed to high humidity conditions during several days.[3] This stability has been attributed to the strength of the carboxylate-Zr bond and to the high connectivity of the metal clusters, $Zr_6O_4(OH)_4(CO_2)_{12}$, which are coordinated by twelve benzenedicarboxylate ligands in the ideal structure (see **Fig. 1**).

This high connectivity can imply the formation of a high concentration of defects, including missing ligands and/or missing clusters, without the collapse of the structure[4-6]. This particularity improves certain desirable properties, like higher surface area, better adsorption and catalytic activity.[7, 8] Therefore, these defects have a key influence on the performances of UiO-66(Zr), and their localization is still highly debated in the literature[6, 9-12]. In particular, when a ligand is missing, it creates coordination vacancies on two adjacent Zr^{4+} ions, and several chemical species, (N,N-dimethylformamide (DMF) solvent, residual water, hydroxide groups and monocarboxylate modulators, such as formate anions) can compete to coordinate these vacancies and ensure electroneutrality. Despite several studies using vibrational spectroscopies, single-crystal X-ray diffraction, elemental analysis and first-principle calculations, the nature of these compensating species remains an unsettled question[6]. Furthermore, it has been shown that DMF and water play an important role in the crystallization of UiO-66(Zr).[6, 13, 14] Nevertheless, the crystallization mechanisms and notably the formation of the secondary building unit from the Zr precursor are not fully understood at atomic level. As a local characterization technique endowed with atomic resolution, solid-state NMR spectroscopy represents a powerful technique to probe the atomic-level structure and dynamics of defects in UiO-66(Zr)[15], the functionalization of the ligands[16, 17], the acidity of these MOFs[18], and the adsorption of guest molecules, such as caffeine[19] and light alkanes[20-22] in these MOFs.

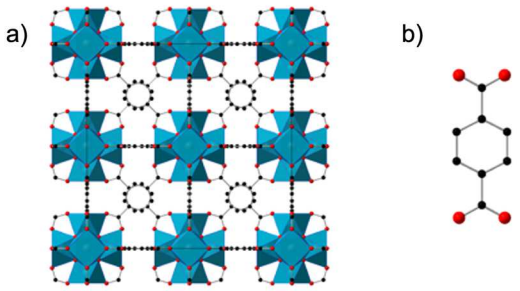

Fig. 1. (a) Crystalline structure of the UiO-66(Zr) MOF along with (b) the structure of the bdc ligand. Color of the atoms: carbon in black, zirconium in blue, and oxygen in red. For sake of clarity, the hydrogen are not represented.

In this work, we investigate the interactions of water and DMF with UiO-66(Zr) using ^{1}H and ^{13}C solid-state NMR spectroscopy. We notably examine the effect of drying on the ^{1}H solid-state NMR spectra. We also demonstrate that UiO-66(Zr) can be selectively deuterated using either deuterated terephthalic acid or deuterated water as a source of deuterium.

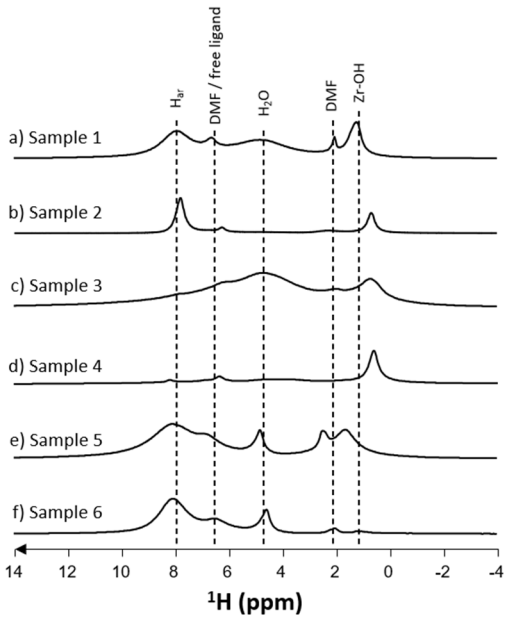

Fig. 2. ^{1}H DEPTH MAS NMR spectra of UiO-66(Zr) of samples (a) **1**, (b) **2**, (c) **3**, (d) **4**, (e) **5** and (f) **6** recorded at room temperature and

B_0 = 9.4 T (except for spectrum **2** recorded at 18.8 T) and MAS frequency ν_r = 12.5 kHz (except for spectra **2** and **4** recorded at ν_r = 20 kHz). Additional experimental details are given in the ESI and in Table **1**. Dotted lines are guides for the eye.

Table 1: Summary of the samples' syntheses and treatment procedures.

Sample	Synthesis	Post-treatment
1	Published procedure [2]	N/A
2		Drying at 100 °C during 16 h
3	Same procedure but using [2,3,5,6-$^2H_4$, $^{17}O_4$]-terephtalic acid as precursor	N/A
4		Drying at 100 °C during 16 h
5	Published procedure[2]	Adsorption of ^2H_2O at 50 °C during 48 h
6		Adsorption of ^2H_2O at 50 °C during 48 h + heating at 100 °C during 16 h

The UiO-66(Zr) MOF was synthesized according to the procedure reported by Cavka *et al*[2] from zirconium(IV) chloride and commercial isotopically unmodified terephtalic acid dissolved in DMF (see section S1 of the Supporting Information). The obtained MOF was then washed with DMF and then ethanol. This procedure aims at removing guest molecules, such as unreacted terephtalic acid and DMF from the pores. The obtained sample denoted **1** (see Table **1**) has a X-ray diffraction pattern similar to that calculated from the crystal structure of UiO-66(Zr)[2] (see Fig. **S9**), which confirms the synthesis of the desired MOF. This sample was packed in an NMR rotor in argon glovebox. Fig. **2a** shows one-dimensional (1D) ^{1}H NMR spectrum under magic-angle spinning (MAS) of sample **1** acquired using DEPTH sequence to remove the broad background ^{1}H signal[23]. This spectrum exhibits a signal near 7.9 ppm assigned to aromatic protons, which agrees with the isotropic chemical shift δ_{iso} = 8.1 ppm calculated for these protons in previous work by density functional theory (DFT) [17] using periodic boundary conditions, CASTEP software[24, 25], projector augmented waves (PAW[26]) and gauge included projector augmented waves (GIPAW[27]) algorithms. The peak at 2.1 ppm is assigned to the methyl protons of DMF, whereas the signal at 6.8 ppm subsumes the contribution of CO(H) group of DMF and carboxylic protons of free terephtalic acid (Table **2**)[28] since its integrated intensity is higher than one sixth of that of the signal at 2.1 ppm. Note that these isotropic chemical shifts are significantly lower than those of DMF in $CDCl_3$. This shielding stems from local magnetic fields by currents in the bdc aromatic rings[29]. The presence of DMF in sample **1** is confirmed by the observation of a resonance at 1660 cm^{-1} corresponding to the stretch of C=O bond of DMF in the Fourier-transformed infrared (FT-IR) spectrum shown in Fig. **S3**. Moreover, one can detect the signals of the DMF in sample **1** besides those of bdc ligand, in the ^{1}H→^{13}C cross-polarization under MAS (CPMAS) spectrum of Fig. **S2a**.

Table 2: Summary of the ^{1}H isotropic chemical shifts and their assignment for the UiO-66 samples **1** to **6**.

	^{1}H δ_{iso} (ppm)	Assignment
Sample **1**	1.3	Zr-OH
	7.9	H_{ar}
	4.9	H_2O
	2.1	DMF (CH_3)
	6.8	DMF (CO)
Sample **2**	0.7	Zr-OH
	7.9	H_{ar}
	4.8	H_2O
	2.0	DMF (CH_3)
	6.2	DMF (CO)
Sample **3**	0.7	Zr-OH
	7.9	H_{ar}
	4.7	H_2O
	2.0	DMF (CH_3)
	6.1	DMF (CO)
Sample **4**	0.6	Zr-OH
	8.2	H_a
	4.6	H_2O
	1.6	DMF (CH_3)
	6.3	DMF (CO)
Sample **5**	1.7	Zr-OH
	8.1	H_{ar}
	4.9	H_2O
	2.5	DMF (CH_3)
	6.9	DMF (CO)
Sample **6**	1.2	Zr-OH
	8.1	H_{ar}
	4.6	H_2O
	2.1	DMF (CH_3)
	6.6	DMF (CO)

The broad peak resonating at 4.9 ppm is assigned to water. This signal is more shielded than in pristine UiO-66(Zr) that does not contain DMF (6 ppm)[17]. This lower isotropic chemical shift attests of longer O<u>H</u>···<u>O</u> distances[30, 31] since DMF can (i) perturb the hydrogen bonds between water molecules and (ii) compete with water for the hydrogen bonding with Zr–OH groups. Finally, the resonance at 1.4 ppm is ascribed to Zr–OH. Its isotropic chemical shift is higher than that calculated by DFT (0.83 ppm) because of the formation of hydrogen bond[17]. However, this value is lower than that of UiO-66(Zr), which does not contain DMF (2.3-2.6 ppm)[17] and where Zr-OH groups are solely bonded to water, since Zr–OH groups form weaker hydrogen bonds with DMF than with water[32]. The formation of hydrogen bond between Zr–OH and DMF is further supported by the observation of cross peaks between Zr–OH protons and DMF ^{13}C signals in the 2D ^{1}H→^{13}C CP-HETCOR NMR spectrum of **1** shown in Fig. **3**. This spectrum also confirms the assignment of ^{1}H DMF signals.

Sample **2** was prepared by drying sample **1** at 100 °C overnight (16 h). As seen in Fig. **S9**, this spectrum exhibits the same diffraction as sample **1**. Hence, the long-range structure of UiO-66(Zr) MOF does not change during the post synthesis thermal treatment. Conversely, it has been shown previously that drying at higher temperature can result in the dihydroxylation of UiO-66(Zr), loss of hydroxyl groups connected to the Zr cluster[33]. As seen in Fig. **2b**, the ^{1}H signal of water vanishes after drying, whereas weak signals of DMF can still be detected (Fig. **S4**). Hence, drying removes most of water molecules but some DMF remains adsorbed in UiO-66(Zr). Nevertheless, the amount of residual DMF is too small to be detected in 1D ^{1}H→^{13}C CPMAS spectrum (see Fig. **S2b**) and by FT-IR (see Fig. **S3b**). Furthermore, the signals of Zr–OH and DMF carbonyl protons are more shielded in sample **2** than in sample **1**. In particular, the δ_{iso} value of Zr–OH in sample **2** (0.6 ppm) is close to that calculated by DFT for an ideal UiO-66(Zr) structure with empty

pore. These observations indicate that the desorption of water suppresses most of the hydrogen bonds for DMF and Zr–OH sites. The residual DMF may be strongly bound to UiO-66(Zr) either by coordinating vacancies on Zr^{4+} ions[14, 34] or by hydrogen bonding with some Zr–OH groups[21, 35]. The narrowing of the aromatic and Zr–OH peaks for sample **2** compared to sample **1** stems from higher MAS frequency and magnetic field strength, which better averages the ^{1}H-^{1}H dipolar interactions, as well as the removal of water and DMF, which reduces these interactions.

In order to simplify the ^{1}H MAS NMR spectrum of UiO-66(Zr), this MOF was also prepared using a deuterated terephtalic acid precursor ([2,3,5,6-$^2H_4$, $^{17}O_4$]-bdc enriched in ^{17}O isotope using mechanochemistry)[36]. The XRD pattern of this sample denoted **3** (see **Table 1**) corresponds to that of UiO-66(Zr). Hence, the desired MOF is synthesized from isotopically labelled terephtalic acid. The ^{1}H MAS NMR spectrum of the sample **3** is displayed in **Fig. 2c**. As expected, the intensity of the aromatic ^{1}H signal is strongly decreased, whereas the signals of Zr–OH, water and DMF are still present. This observation indicates that this synthetic route results in the selective deuteration of the ligands of UiO-66(Zr). Contrary to sample **1**, the water signal is more intense than the other peaks. This large water signal evidences a larger amount of adsorbed water, which results in larger ^{1}H-^{1}H dipolar interactions and hence, broader lines. Surprisingly the Zr-OH signal is more shielded in sample **3** than in sample **1**. This shift suggests different hydrogen bonds between Zr-OH group and guest molecules between the two samples. Sample **3** is synthesized from terephtalic acid prepared by mechanochemistry, instead of commercial terephtalic acid for sample **1**. This difference affects the crystallization of the MOF, notably the crystallite size, and hence, the removal of guest molecules during the activation.

Drying at 100 °C overnight of sample **3** does not alter the crystalline structure of UiO-66(Zr), as seen in **Fig. S9**, but removes most of water and DMF molecules from the pores. The ^{1}H NMR spectrum of the obtained sample denoted **4** is dominated by the signal of Zr–OH groups (see Fig. **2d**). Nevertheless, signals of residual water and DMF are detected (see Fig. **S5**). A weak signal ascribed to partially protonated bdc ligands is also visible.

In order to decrease the ^{1}H NMR signal of water, deuterated water was adsorbed in sample **1**. The crystalline structure of UiO-66(Zr) is preserved, as seen in **Fig. S9**, owing to the good stability of this MOF in presence of water[3]. The ^{1}H NMR spectrum of the obtained sample denoted **5** is shown in **Fig. 2e** and exhibits a narrower water signal than for sample **1,** since most of water molecules are deuterated, which results in reduced ^{1}H-^{1}H dipolar interactions. Because of the adsorption of water, UiO-66(Zr) pores of sample **5** contain a higher amount of water than those of sample **1**, even if these deuterated water molecules are not detected on the ^{1}H NMR spectrum. This higher uptake leads to an increased number of hydrogen bonds between water and Zr–OH groups as well as between water and DMF and hence, the deshielding of the ^{1}H signals of Zr–OH groups as well as DMF. Moreover, the presence of this signal reveals that a significant fraction of the Zr-OH is not deuterated. The δ_{iso} values of bdc and DMF (CO(H)) protons are similar in samples **1** and **5** (compare **Fig. 2a** and **2e**). Hence, the adsorption of water does not significantly alter the structure of UiO-66(Zr)[2]. However, a deshielded methyl DMF is observed in sample **5**. This could be assigned to the presence of the connected Zr-OD and D_2O.

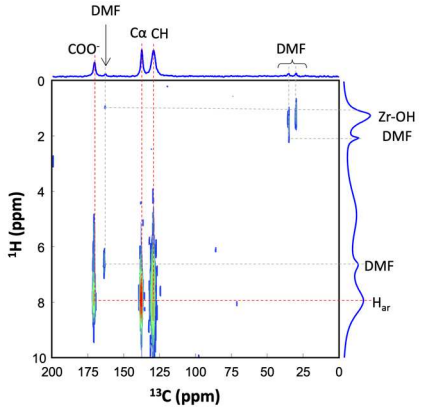

Fig. 3. 2D ^{1}H→^{13}C CP-HETCOR NMR spectrum of **1** at B_0 = 9.4 T with ν_r = 12.5 kHz. Spectra on the top and on the right correspond to the 1D ^{1}H→^{13}C CPMAS and ^{1}H MAS NMR spectra of Figs. **2a** and **S2a**, respectively.

The UiO-66(Zr) structure is preserved when heating sample **5** overnight at 100 °C (leading to sample **6**), as seen in **Fig. S9**, again showing the high stability of this MOF at high temperature in the presence of water. This post-treatment decreases the ^{1}H NMR signals of DMF and water. Nevertheless, the intensities of these peaks remain higher than for samples **2** and **4** since the amount of adsorbed water in sample **5** was higher than in samples **1** and **3**. Nevertheless, this post-treatment leads to the deuteration

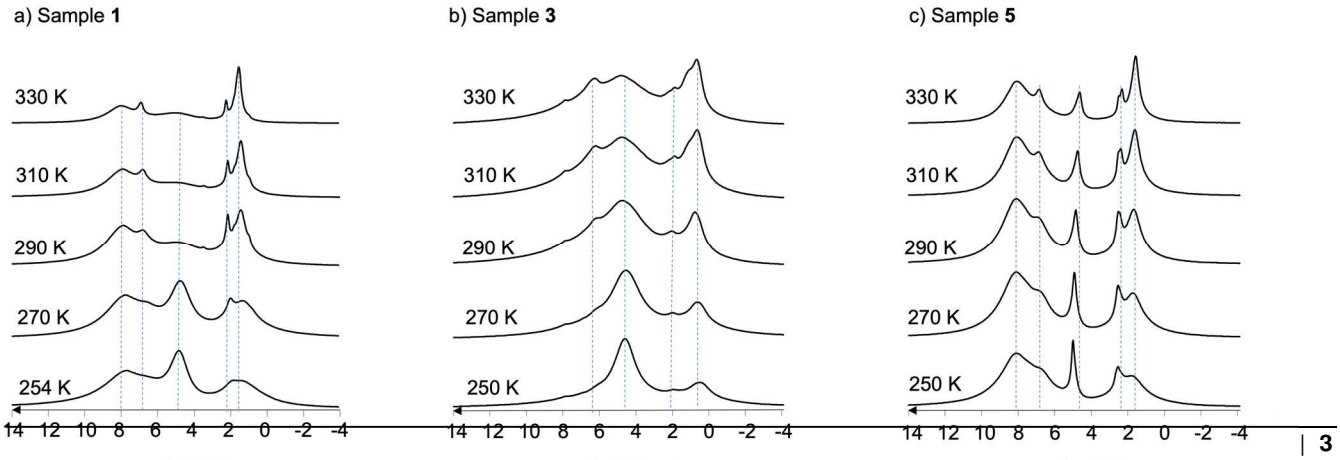

Fig. 4. ^{1}H DEPTH MAS NMR spectra of UiO-66(Zr) of samples (a) **1**, (b) **3** and (c) **5** at different temperatures (indicated on the figure) at B_0 = 9.4 T with ν_r = 12.5 kHz. Additional experimental details are given in the ESI.

of Zr–OH groups by hydrogen exchange with deuterated water. The δ_{iso} value of residual protonated Zr–OH group for sample **6** is close to that measured for sample **1**. This observation is consistent with the fact that these two samples still contain a significant fraction of adsorbed DMF and water.

We also recorded the 1D ^{1}H MAS NMR spectra of samples **1**, **3** and **5** at different temperatures, as shown in Fig. **4**. The variations of ^{1}H isotropic chemical shifts as function of temperature for samples **1**, **3** and **5** are shown in **Figs. S6, S7** and **S8**, respectively. No coalescence of water and Zr-OH signals is observed at 330 K for these three samples. This observation indicates that the chemical exchange between these protons is much slower than 1.4×10^{3} s^{-1} at 330 K. Furthermore, for these three samples, the resonances of aromatic protons, DMF and Zr–OH narrow at higher temperature because of increased atomic-level dynamics, including 180° flips and libration of the phenylene rings, which better average out the ^{1}H-^{1}H dipolar couplings[37, 38]. For sample **1**, this line narrowing allows resolving a shoulder near 1 ppm, which is ascribed to Zr-OH groups involved in weak hydrogen bonds with isotropic chemical shift close to those calculated by DFT for Zr-OH protons in UiO-66(Zr) without guest molecules in the pores[17]. These weakly bonded Zr-OH groups are not observed for samples **3** and **5**, which contains a larger amount of adsorbed water. Conversely the water signals broaden at higher temperature. A possible explanation is that at higher temperature, the tumbling of water molecules is faster and the correlation time of this motion becomes comparable to the rotor period. Consequently, interference effects occur between the sample spinning and the water dynamics, which prevents the refocusing of ^{1}H-^{1}H dipolar interaction by MAS and hence, results in a broadening of the NMR signal[39]. The signal of water protons is narrower for sample **5** since a large fraction of the water molecules is deuterated and hence, the protonated water molecules are subject to smaller ^{1}H-^{1}H dipolar interaction. At high temperature (330 K) for samples **3** and **5**, methyl signal is split, which suggest a partial decomposition of DMF into dimethylamine. This hydrolysis is not observed for sample **1**, which contains a lower amount of water.

In summary, we observed using ^{1}H and ^{13}C MAS NMR bound DMF and water in UiO-66(Zr). 2D ^{1}H→^{13}C HETCOR spectrum shows the formation of hydrogen bonds between DMF and Zr–OH groups. Furthermore, ^{1}H NMR data indicate that connected water is hydrogen bonded to Zr–OH groups. We also demonstrate the possibility to deuterate selectively the UiO-66(Zr) by using deuterated terephthalic acid as precursor or by hydrogen exchange with deuterated water.

The Chevreul Institute is thanked for its help in the development of this work through the ARCHI-CM project supported by the "Ministère de l'Enseignement Supérieur de la Recherche et de l'Innovation", the region "Hauts-de-France", the ERDF program of the European Union and the "Métropole Européenne de Lille". Financial support from the contract Isite ULNE: MOFFiN-OPE-2019-43-5400 and is gratefully acknowledged. Danielle Laurencin is acknowledged for providing the deuterated terephtalic acid.

Notes and references

[a] *Univ. Lille, CNRS, Centrale Lille, Univ. Artois, UMR 8181 – UCCS – Unité de Catalyse et Chimie du Solide, F-59000 Lille, France.*
frederique.pourpoint@centralelille.fr

† Electronic Supplementary Information (ESI) available: [Experimental details, ^{13}C CPMAS NMR and IR spectra of samples **1** and **2**, ^{1}H MAS NMR of sample **2**].

1. Y. Bai, Y. B. Dou, L. H. Xie, W. Rutledge, J. R. Li and H. C. Zhou, *Chem. Soc. Rev.*, 2016, **45**, 2327-2367.
2. J. H. Cavka, S. Jakobsen, U. Olsbye, N. Guillou, C. Lamberti, S. Bordiga and K. P. Lillerud, *J. Am. Chem. Soc.*, 2008, **130**, 13850-13851.
3. J. B. DeCoste, G. W. Peterson, H. Jasuja, T. G. Glover, Y. G. Huang and K. S. Walton, *J. Mater. Chem. A*, 2013, **1**, 5642-5650.
4. H. Wu, Y. S. Chua, V. Krungleviciute, M. Tyagi, P. Chen, T. Yildirim and W. Zhou, *J. Am. Chem. Soc.*, 2013, **135**, 10525-10532.
5. G. C. Shearer, S. Chavan, S. Bordiga, S. Svelle, U. Olsbye and K. P. Lillerud, *Chem. Mater.*, 2016, **28**, 3749-3761.
6. M. Taddei, *Coord. Chem. Rev.*, 2017, **343**, 1-24.
7. P. Ghosh, Y. J. Colon and R. Q. Snurr, *Chem. Commun.*, 2014, **50**, 11329-11331.
8. W. B. Liang, C. J. Coghlan, F. Ragon, M. Rubio-Martinez, D. M. D'Alessandro and R. Babarao, *Dalton Trans.*, 2016, **45**, 4496-4500.
9. K. Tan, H. Pandey, H. Wang, E. Velasco, K. Y. Wang, H. C. Zhou, J. Li and T. Thonhauser, *J. Am. Chem. Soc.*, 2021, **143**, 6328-6332.
10. C. A. Trickett, K. J. Gagnon, S. Lee, F. Gandara, H. B. Burgi and O. M. Yaghi, *Angew. Chem.-Int. Ed.*, 2015, **54**, 11162-11167.
11. M. Vandichel, J. Hajek, F. Vermoortele, M. Waroquier, D. E. De Vos and V. Van Speybroeck, *CrystEngComm*, 2015, **17**, 395-406.
12. J. K. Bristow, K. L. Svane, D. Tiana, J. M. Skelton, J. D. Gale and A. Walsh, *J. Phys. Chem. C*, 2016, **120**, 9276-9281.
13. M. Taddei, K. C. Dumbgen, J. A. van Bokhoven and M. Ranocchiari, *Chem. Commun.*, 2016, **52**, 6411-6414.
14. M. Taddei, J. A. van Bokhoven and M. Ranocchiari, *Inorg. Chem.*, 2020, **59**, 7860-7868.
15. Y. Fu, Z. Z. Kang, J. L. Yin, W. C. Cao, Y. Q. Tu, Q. Wang and X. Q. Kong, *Nano Lett.*, 2019, **19**, 1618-1624.
16. J. Tang, S. H. Li, Y. C. Su, Y. Y. Chu, J. Xu and F. Deng, *J. Phys. Chem. C*, 2020, **124**, 17640-17647.
17. S. Devautour-Vinot, G. Maurin, C. Serre, P. Horcajada, D. P. da Cunha, V. Guillerm, E. D. Costa, F. Taulelle and C. Martineau, *Chem. Mater.*, 2012, **24**, 2168-2177.
18. J. Tang, S. H. Li, Y. Y. Chui, Y. Q. Xiao, J. Xu and F. Deng, *Magn. Reson. Chem.*, 2019, 1-8.
19. S. Devautour-Vinot, C. Martineau, S. Diaby, M. Ben-Yahia, S. Miller, C. Serre, P. Horcajada, D. Cunha, F. Taulelle and G. Maurin, *J. Phys. Chem. C*, 2013, **117**, 11694-11704.
20. Y. Q. Xiao, Y. Y. Chu, S. H. Li, Y. C. Su, J. Tang, J. Xu and F. Deng, *J. Phys. Chem. C*, 2020, **124**, 3738-3746.
21. Y. An, A. Kleinhammes, P. Doyle, E. Y. Chen, Y. Song, A. J. Morris, B. Gibbons, M. Cai, J. K. Johnson, P. B. Shukla, M. N. Vo, X. Wei, C. E. Wilmer, J. P. Ruffley, L. L. Huang, T. M. Tovar, J. J. Mahle, C. J. Karwacki and Y. Wu, *J. Phys. Chem. Lett.*, 2021, **12**, 892-899.
22. A. E. Khudozhitkov, S. S. Arzumanov, D. I. Kolokolov and A. G. Stepanov, *J. Phys. Chem. C*, 2021, **125**, 13391-13400.
23. D. G. Cory and W. M. Ritchey, *J. Magn. Reson.*, 1988, **80**, 128-132.
24. S. J. Clark, M. D. Segall, C. J. Pickard, P. J. Hasnip, M. J. Probert, K. Refson and M. C. Payne, *Zeitschrift Fur Kristallographie*, 2005, **220**, 567-570.
25. M. D. Segall, P. J. D. Lindan, M. J. Probert, C. J. Pickard, P. J. Hasnip, S. J. Clark and M. C. Payne, *Journal of Physics-Condensed Matter*, 2002, **14**, 2717-2744.
26. M. Profeta, F. Mauri and C. J. Pickard, *J. Am. Chem. Soc.*, 2003, **125**, 541-548.

27. C. J. Pickard and F. Mauri, *Phys. Rev. B*, 2001, **63**, 245101(245101-245113).
28. C. Volkringer, M. Meddouri, T. Loiseau, N. Guillou, J. Marrot, G. Férey, M. Haouas, F. Taulelle, N. Audebrand and M. Latroche, *Inorg. Chem.*, 2008, **47**, 11892-11901.
29. A. Nandy, A. C. Forse, V. J. Witherspoon and J. A. Reimer, *J. Phys. Chem. C*, 2018, **122**, 8295-8305.
30. H. Eckert, J. P. Yesinowski, L. A. Silver and E. M. Stolper, *J. Phys. Chem.*, 1988, **92**, 2055-2064.
31. C. Gervais, C. Coelho, T. Azais, J. Maquet, G. Laurent, F. Pourpoint, C. Bonhomme, P. Florian, B. Alonso, G. Guerrero, P. H. Mutin and F. Mauri, *J. Magn. Reson.*, 2007, **187**, 131-140.
32. T. Steiner, *Angew. Chem.-Int. Ed.*, 2002, **41**, 48-76.
33. G. C. Shearer, S. Forselv, S. Chavan, S. Bordiga, K. Mathisen, M. Bjorgen, S. Svelle and K. P. Lillerud, *Top. Catal.*, 2013, **56**, 770-782.
34. S. Oien, D. Wragg, H. Reinsch, S. Svelle, S. Bordiga, C. Lamberti and K. P. Lillerud, *Cryst. Growth Des.*, 2014, **14**, 5370-5372.
35. S. Wang, J. S. Lee, M. Wahiduzzaman, J. Park, M. Muschi, C. Martineau-Corcos, A. Tissot, K. H. Cho, J. Marrot, W. Shepard, G. Maurin, J. S. Chang and C. Serre, *Nat. Energy*, 2018, **3**, 985-993.
36. C. H. Chen, I. Goldberga, P. Gaveau, S. Mittelette, J. Spackova, C. Mullen, I. Petit, T. X. Metro, B. Alonso, C. Gervais and D. Laurencin, *Magn. Reson. Chem.*, 2021.
37. D. I. Kolokolov, A. G. Stepanov, V. Guillerm, C. Serre, B. Frick and H. Jobic, *J. Phys. Chem. C*, 2012, **116**, 12131-12136.
38. A. E. Khudozhitkov, D. I. Kolokolov and A. G. Stepanov, *J. Phys. Chem. C*, 2018, **122**, 12956-12962.
39. P. Hodgkinson, *Intramolecular Motion in Crystalline Organic Solids*, eMagRes, 2008.